The microtubule plus-end tracking protein Bik1 is required for chromosome congression

Alexander Julner [1], Marjan Abbasi [1], and Victoria Menéndez-Benito [1,2]

[1] Department of Biosciences and Nutrition, Karolinska Institutet, SE-141 83, Huddinge, Sweden.

[2] Correspondence: victoria.menendez.benito@ki.se

RUNNING HEAD: Bik1 controls chromosome congression

ABBREVIATIONS: Adenosine triphosphate (ATP); nuclear export signal (NES); spindle pole body (SPB); microtubule plus-end tracking proteins (+TIPs); superfolder GFP (sfGFP); bimolecular fluorescence complementation (BiFC).

Number of characters: 16815

Abstract

During mitosis, sister chromatids congress on both sides of the spindle equator to facilitate the correct partitioning of the genomic material. Chromosome congression requires a finely tuned control of microtubule dynamics by the kinesin motor proteins. In *Saccharomyces cerevisiae*, the kinesin proteins Cin8, Kip1, and Kip3 have a pivotal role in chromosome congression. It has been hypothesized that additional proteins that modulate microtubule dynamics are also involved. Here, we show that the microtubule plus-end tracking protein Bik1 – the budding yeast ortholog of CLIP-170 – is essential for chromosome congression. We find that nuclear Bik1 localizes to the kinetochores in a cell-cycle-dependent manner. Disrupting the nuclear pool of Bik1 with a nuclear export signal (Bik1-NES) leads to a slower cell cycle progression characterized by a delayed metaphase-anaphase transition. Bik1-NES cells have mispositioned kinetochores along the spindle in metaphase. Furthermore, using proximity-dependent methods, we identify Cin8 as an interaction partner of Bik1. Deleting CIN8 reduces the amount of Bik1 at the spindle. In contrast, Cin8 retains its typical bilobed distribution in the Bik1-NES mutant and does not localize to the unclustered kinetochores. Thus, we propose that Bik1 functions with Cin8 to regulate kinetochore-microtubule dynamics for correct kinetochore positioning and chromosome congression.

Keywords: mitosis, kinetochore, chromosome, kinesins, genetic stability.

35 # Introduction

36 Cell division relies on the accurate segregation of sister chromatids to generate functional daughter
37 cells. Before segregation, sister chromatids are positioned at the spindle equator through a process
38 known as chromosome congression that culminates with the metaphase plate formation in
39 metazoans (reviewed in (Maiato et al., 2017)). The establishment of a metaphase plate forces all the
40 chromosomes to segregate from the same starting position, thereby contributing to faithful
41 segregation. Despite the relevance of chromosome congression, its molecular mechanisms remain
42 unclear.
43
44 The budding yeast *Saccharomyces cerevisiae* is an appealing model organism to study spindle
45 dynamics because it is amenable to genetic engineering and has a relatively simple spindle. Budding
46 yeast has 16 chromosomes. After duplication, each sister chromatid is linked by a kinetochore to a
47 single kinetochore microtubule emanating from the spindle pole body (SPB), the yeast centrosome
48 (Winey & O'Toole, 2001). Each SPB also gives rise to a few interpolar microtubules (starting with
49 around six and ending with two interpolar microtubules from each SPB), with plus-ends that overlap
50 at the middle of the spindle (O'Toole et al., 1999; Peterson & Ris, 1976; Winey et al., 1995). In
51 prometaphase, kinetochores congress in two opposite clusters near the spindle equator, equidistant
52 from the SPBs. As in metazoan cells, this appears to occur prior to biorientation of sister chromatids
53 (Marco et al., 2013).
54
55 Several studies have shown that kinetochore microtubules are regulated in a length-dependent
56 manner (Gardner et al., 2005; Pearson et al., 2006; Sprague et al., 2003). Short microtubules tend to
57 grow, whereas long microtubules that extend towards the spindle equator are destabilized and
58 depolymerize. As sister chromatids are held together by cohesin, depolymerization of kinetochore
59 microtubules generates tension, mediated by the Ndc80 and Dam1 complexes' ability to track the
60 dynamic tips of the kinetochore microtubules (Powers *et al.*, 2009; Suzuki *et al.*, 2016).

61 Kinesin motors – proteins that move along microtubules powered by the hydrolysis of adenosine
62 triphosphate (ATP) – are involved in chromosome congression in several organisms (see Maiato *et*
63 *al.*, 2017, Table 1). In budding yeast, the deletion of the kinesins Cin8, Kip3, and, to a lesser extent,
64 Kip1, results in declustering of kinetochores (Gardner et al., 2008; Marco et al., 2013; Tytell & Sorger,
65 2006; Wargacki et al., 2010). Cin8 and Kip3 have been shown to act as length-dependent microtubule
66 depolymerases, promoting catastrophe of long microtubules (Gardner et al., 2008; Su et al., 2011;
67 Varga et al., 2006).
68
69 It has long been speculated that other microtubule-associated proteins could play a role in
70 chromosome congression (Kops *et al.*, 2010). Specifically, microtubule plus-end tracking proteins
71 (+TIPs) are interesting candidates, because they accumulate at kinetochore microtubule plus-ends
72 and regulate their dynamics (reviewed in Akhmanova & Steinmetz, 2010). Bik1, the yeast ortholog of
73 CLIP-170, is a +TIP protein that exists in cytoplasmic and nuclear pools within the cell (Carvalho et al.,
74 2004). The cytoplasmic pool is important for mitotic spindle positioning through both the Kar9 and
75 the dynein pathways (reviewed in Miller *et al.*, 2006). First, Bik1 promotes phosphorylation of Kar9
76 for asymmetric localization at the old SPB (Moore et al., 2006). Kar9, together with the +TIP protein
77 Bim1 and the actin-guided myosin motor protein Myo2, mediates the capture of astral microtubules
78 at the bud cortex, contributing to spindle alignment and nuclear migration (Xiang, 2018). During
79 anaphase, Bik1 is transported by the kinesin Kip2 to the plus-ends of astral microtubules, where it
80 facilitates the recruitment of dynein (Carvalho *et al.*, 2004; Roberts *et al.*, 2014). Dynein is a minus
81 end-directed motor and will pull the spindle resulting in nuclear migration to the bud.
82
83 The nuclear pool of Bik1 is associated with the spindle at SPBs and kinetochores (Carvalho et al.,
84 2004; Lin et al., 2001), but its function is not well understood. Early studies found that deleting BIK1
85 results in cells with short or non-detectable astral microtubules (Berlin *et al.*, 1990). In contrast, cells
86 overexpressing Bik1 display short spindle microtubules and long astral microtubules. In this study,

87 we investigate the nuclear function of Bik1 and its role in chromosome congression and cell cycle
88 progression.
89

90 Results and discussion

91 Bik1 localizes to kinetochores in a cell cycle-dependent manner

92 To better understand the nuclear pool of Bik1, we first explored the localization of the protein at
93 different stages of the cell cycle. We used cells expressing Bik1-superfolder GFP (sfGFP), mTurquoise-
94 Tub1 (alpha tubulin, microtubule marker), and either Ndc80-tagRFPT (kinetochore marker) or Spc42-
95 tagRFPT (SPB marker) (Figure 1A). In metaphase cells, nuclear Bik1 was primarily found between SPBs
96 and overlapping with kinetochores. This bilobed kinetochore-associated distribution has also been
97 reported for the kinesins Cin8, Kip1, and Kip3 (Gardner et al., 2008; Tytell & Sorger, 2006; Wargacki
98 et al., 2010). Anaphase cells, on the other hand, displayed nuclear Bik1 concentrated in patches
99 along interpolar microtubules, again similar to what is reported for kinesins Cin8, Kip1, and Kip3.
100 Cytoplasmic Bik1, meanwhile, was localized to astral microtubule tips at the cell cortex.
101

102 To confirm the metaphase association with kinetochores, we used cells expressing the APC/C co-
103 activator Cdc20 under the control of the galactose inducible *GAL1* promoter. Shifting the carbon
104 source from galactose to glucose represses the expression of CDC20 and thereby arrests the cells at
105 the metaphase-to-anaphase transition. Bik1-sfGFP was localized at kinetochore clusters in
106 metaphase arrested cells (Figure 1B), confirming what we observed in cycling cells with short
107 spindles. In summary, we conclude that Bik1 associates with kinetochores from G1 until metaphase,
108 after which it instead is localized to interpolar microtubules.
109

110 Nuclear Bik1 is needed for timely cell cycle progression

111 Bik1 in the cytoplasm localizes to astral microtubules and plays an important role in mitotic spindle
112 positioning (Carvalho et al., 2004; Moore et al., 2006). To disrupt the kinetochore function of Bik1
113 while maintaining its cytoplasmic function, we fused a strong nuclear export consensus sequence
114 (NES) (Kosugi et al., 2008) to the C-terminal end of Bik1-sfGFP or Bik1-5xFlag (collectively referred to
115 as Bik1-NES, Figure 1C). We imaged Bik1-NES cells expressing mTurquoise-Tub1, and Nc80-tagRFPT
116 and confirmed that the mutant indeed excludes Bik1 from the nucleus while maintaining its
117 localization at astral microtubules (Figure 1D). To quantify the effectiveness of the NES, we followed
118 the localization of Bik1 in Bik1-sfGFP and Bik1-sfGFP-NES cells expressing mTurquoise-Tub1. We
119 synchronized the cells in G1 with α-factor, released them in fresh media, and fixed cells at 10-minute
120 intervals from release. We then measured Bik1 intensity along the spindle in metaphase cells and
121 found that, as expected, Bik1-NES cells have significantly less sfGFP signal at the spindle microtubules
122 than Bik1 cells (Figure 1E).

123

124 We next assessed cell cycle progression in the absence of nuclear Bik1. We synchronized Bik1-sfGFP
125 and Bik1-sfGFP-NES cells in G1 with α-factor and scored the number of cells in G1/S, metaphase, or
126 anaphase according to the spindle length (mRuby2-Tub1) (Figure 2A). The strain expressing Bik1-
127 sfGFP had a sharp peak of metaphase cells at 40 min and a high number of cells with long spindles
128 50-60 min after the release. Bik1-sfGFP-NES cells, by contrast, displayed a broader peak of
129 metaphase cells that spans between 40-60 min post-release and a 10 min delay in the anaphase
130 peak.

131

132 We then examined Bik1-sfGFP and Bik1-sfGFP-NES cells after G1 synchronization with α-factor by
133 time-lapse imaging (Figure 2B-E). In the Bik1-sfGFP strain, Bik1 was localized to the kinetochores
134 from G1 through metaphase. When the spindle elongates in anaphase, Bik1 was no longer associated
135 with the kinetochores and was found in patches along the interpolar microtubules instead (Figure

136 2B-C), as observed in fixed cells (Figure 1 A). The fluorescence intensity of Bik1-sfGFP at kinetochores
137 was highest at metaphase when kinetochores cluster and reduced to near background levels in
138 anaphase (Figure 2D). In agreement with the cell-cycle analysis from fixed cells, we observed a slight
139 delay in cell cycle progression in Bik1-NES cells (Figure 2B, arrows). Our quantifications showed that
140 the time from the appearance of two kinetochore clusters to their segregation into mother and
141 daughter cells is approximately 10 min longer in Bik1-NES cells (Figure 2E). Interestingly, we
142 occasionally observed all kinetochores of short spindles transferred to the daughter cell in the NES
143 mutant strain before elongation occurred (Figure 2 B, 15 min and 25-30 min). We interpret this as a
144 secondary effect of the prolonged metaphase of the mutant.
145
146 Cells lacking nuclear Bik1 display aberrant kinetochore positioning
147 Because Bik1 localizes near the kinetochores in metaphase, we hypothesized that the prolonged
148 metaphase of Bik1-NES cells might be due to a dysregulation in kinetochore clustering. To test this
149 hypothesis, we analyzed the distribution of the kinetochore component Ndc80-sfGFP relative to the
150 SPBs (Spc42-tagRFPT) in cells expressing either Bik1-5xFlag or Bik1-5xFlag-NES arrested in metaphase
151 (PGal1-Cdc20) (Figure 3). While Bik1-5xFlag cells showed typical Ndc80 clusters, we observed cells
152 with long stretches of Ndc80 in the Bik1-5xFlag-NES mutant (Figures 3A-B). The unclustered
153 kinetochore phenotype was observed in 60% of the Bik1-NES metaphase cells (Figure 3C). Line scan
154 analysis of the Ndc80-sfGFP fluorescence relative to the SPBs showed that Bik1-NES cells have a
155 flattened distribution of Ndc80 with kinetochores mispositioned towards the spindle equator (Figure
156 3D).
157
158 Bik1 has previously been suggested to contribute to the kinetochore-microtubule attachment. Bik1 is
159 needed to nucleate microtubules that capture kinetochores after centromere re-activation (Tanaka
160 et al., 2005). Furthermore, a binding partner of Bik1, the +TIP Bim1, was recently shown to promote
161 *in vitro* oligomerization of Dam1 complexes– a major component of the yeast outer kinetochore

162 (Dudziak et al., 2021). Therefore, Bik1's function in kinetochore end-on attachment could contribute
163 to the cell cycle delay we observe. Yet, we did not detect unattached kinetochores in the Bik1-NES
164 mutant. Instead, the kinetochores are aligned in the spindle but appear unclustered during
165 metaphase.
166
167 Previous studies have shown that the kinesins Cin8 and to a lesser extent Kip1 and Kip3 are required
168 for yeast chromosome congression (Gardner et al., 2008; Tytell & Sorger, 2006; Wargacki et al.,
169 2010). However, the deletion of each kinesin results in slightly different types of clustering defects. In
170 the cin8Δ mutant, the kinetochores are positioned closer to the spindle equator (Gardner et al.,
171 2008; Tytell & Sorger, 2006; Wargacki et al., 2010). The kip1Δ mutant has a similar, but weaker,
172 phenotype (Gardner et al., 2008; Tytell & Sorger, 2006). Conversely, Ndc80 clusters in kip3Δ cells
173 appear closer towards the spindle poles (Wargacki et al., 2010). We found that the Ndc80 foci in the
174 Bik1-NES mutant appear shifted towards the spindle equator (Figure 3D), as has been reported for
175 cin8Δ cells.
176
177 Bik1 interacts with Cin8 at the spindle
178 To investigate Bik1's association with kinesins, we performed single-step affinity purification of Bik1-
179 Flag in metaphase arrested cells, followed by mass spectrometry analysis. Bik1-Flag co-purified with
180 the yeast kinesins Kip2, Cin8, Kip1, Kip3 and Kar3 (Table 1). Notably, the kinesin Cin8 appeared with a
181 similar coverage as the known interactor Kip2 (Supplementary data S1).
182
183 The defect of Bik1-NES cells in kinetochore clustering shown in Figure 3A phenocopies CIN8 deletion
184 (Gardner et al., 2008; Tytell & Sorger, 2006; Wargacki et al., 2010). Therefore, we decided to study
185 the Bik1-Cin8 interaction in more detail. We investigated whether Cin8 and Bik1 interact *in vivo*
186 using proximity-dependent biotin identification (TurboID), a proximity labelling assay that can detect
187 transient or weak protein-protein interactions (Roux et al., 2012). We fused TurboID, a mutated

188 version of a bacterial biotin ligase BirA (Branon et al., 2018; Larochelle et al., 2019), to the C-terminus
189 of Bik1 (Figure 4A). We then Flag-tagged Cin8 or Kip2, a kinesin that interacts with Bik1 at astral
190 microtubules (Carvalho et al., 2004). Both Cin8 and Kip2 were recovered after streptavidin pulldown
191 when expressed in Bik1-TurboID cells, indicating that Bik1 and Cin8 are in proximity *in vivo* (Figure
192 4B).
193
194 We next looked at the interaction between Bik1 and Cin8 in individual cells by bimolecular
195 fluorescence complementation (BiFC) (Sung & Huh, 2007). Briefly, an N-terminal fragment of the
196 yellow fluorescent protein Venus was fused to the C-terminus of Bik1, and a complimentary C-
197 terminal Venus fragment was fused to the C-terminus of Cin8. We detected BiFC signal at the spindle,
198 predominantly in metaphase and anaphase cells (Figure 4 C-D). Interestingly, the BiFC signal in
199 metaphase cells appeared as 1-2 dots at the spindle, while the signal in anaphase cells appeared as a
200 single dot around the spindle midzone (Figure 4 C).
201
202 We then investigated the dependence of Cin8 and Bik1 to localize to the spindle. In the Bik1-NES
203 mutant, Cin8 still forms two foci between SPBs and kinetochores (Figure 5A and B), even in cells with
204 unclustered kinetochores. This result was surprising as Cin8 has been shown to bind kinetochores
205 directly (Suzuki et al., 2018). Linescan analysis of Cin8-sfGFP localization in relation to SPBs showed
206 that Cin8 localization is unaltered in the absence of nuclear Bik1 (Figure 5B). Deletion of CIN8, on the
207 other hand, resulted in a significantly reduced Bik1 intensity at the spindle (Figure 5C-D). Overall,
208 these data suggest that a portion of nuclear Bik1 associates with and is dependent on Cin8 to bind
209 the spindle.
210
211 The reduced Bik1 recruitment to the spindle and kinetochores explains why Bik1 cannot compensate
212 for the lack of Cin8, which is known to cause severe defects in assembling the mitotic spindle (Hoyt et
213 al., 1992; Kotwaliwale et al., 2007). A previous study has shown that Cin8 mediates chromosome

214 congression by depolymerizing kinetochore microtubules in a length-dependent manner (Gardner et
215 al., 2008). Gardner and coworkers proposed that Cin8 binds randomly to kinetochore microtubules
216 and walks towards the plus-end to promote microtubule plus-end disassembly directly. However, in
217 Bik1-NES cells, Cin8 is insufficient to regulate chromosome congression. Moreover, Cin8 does not
218 localize to the unclustered kinetochores in the Bik1-NES mutant. Taken together, these observations
219 suggest that Bik1 is a binding partner of Cin8 that contributes to the disassembly of kinetochore
220 microtubules to achieve chromosome congression at metaphase. There are at least two other
221 examples where plus-end directed kinesin motors interact with Bik1. Kip2 transports Bik1 to astral
222 microtubule plus ends to ensure proper spindle alignment (Carvalho et al., 2004; Caudron et al.,
223 2008). Furthermore, it has been suggested that Bik1 and Kar3 form a complex at the junction of
224 oppositely oriented MTs during mating to induce microtubule depolymerization for nuclear
225 congression to occur (Molk et al., 2006).
226
227 We propose that Bik1 increases the processivity of Cin8. Bik1 has been suggested to be a processivity
228 factor for the kinesin Kip2 at astral microtubules (Hibbel et al., 2015). Likewise, Bik1 might be needed
229 for Cin8 to reach the plus-ends of long kinetochore microtubules that extend beyond bundled
230 kinetochore microtubules. Cin8 is a bidirectional kinesin and *in vitro* studies have shown it
231 preferentially moves in a minus-end directed manner as single motors (Gerson-Gurwitz et al., 2011;
232 Pandey et al., 2021; Roostalu et al., 2011). Directional switching occurs when Cin8 motors are
233 clustered (Pandey et al., 2021; Roostalu et al., 2011), and other kinesin-5 motors switch directionality
234 in response to steric crowding on MTs (Britto et al., 2016). Loss of nuclear Bik1 could therefore lead
235 to ineffective plus-end directed movement of Cin8 on long kinetochore microtubules and failure to
236 cluster kinetochores at metaphase. This is supported by the observation that Cin8 is not localized
237 along rod-like distribution of Ndc80 in the Bik1-NES mutant.

238 # Materials and Methods

239 ## Yeast strains and plasmids

240 All *S. cerevisiae* strains used in this study are derivatives of BY4741 and are listed in Table S1. The
241 epitope tagged alleles (sfGFP and tagRFPT), TurboID-3xmyc and BiFC were constructed at the
242 endogenous loci by standard PCR-based integration as described in (Longtine et al., 1998) and
243 confirmed by PCR, sequencing and microscopy. The plasmids used to generate the strains are listed
244 in Table S2. Strains with fluorescently tagged Tub1 were constructed as described in (Markus et al.,
245 2015). Briefly, the listed plasmids were linearized using BsaBI (New England Biolabs, R0537S) and
246 integrated at the endogenous TUB1 locus by homologous recombination.

247

248 ## Growth conditions

249 Cells were grown at 30°C in YEP (1% yeast extract, 2% bacto-peptone) medium supplemented with
250 2% glucose (YEPD) unless otherwise stated. For G1 arrest, overnight cultures were diluted to OD_{600} =
251 0.1 in fresh media, grown for 2.5 hours and arrested by adding 3 µg/ml α-factor (Sigma, custom
252 peptide WHWLQLKPGQPMY) every 60 min for 120 min. Cells were released by washing away α-factor
253 with 1x culture volume of YEPD and resuspending in 1x culture volume of YEPD, and further grown at
254 30°C. For metaphase arrest, PGal1-Cdc20 cells were grown in YEP supplemented with 2% raffinose
255 and 2% galactose, and switched to YEPD for 120 min.

256

257 ## Fluorescence imaging

258 Cells were fixed in 4% formaldehyde on ice for 60 minutes, washed with PBS and stored in PBS at 4°C
259 until imaging. Cells were imaged in concanavalin A-coated 96 well glass bottom plates. Images were
260 acquired using a Nikon Ti microscope, equipped with a Zyla 4.2+ sCMOS camera and a 60x water
261 immersion objective (NA 1.2). Z-stack images were captured for fixed cells, as described in the figure

262 legends. Images for BiFC and immunofluorescence were acquired using a Nikon Ti2 microscope,
263 equipped with a Prime BSI sCMOS camera and a 60x water immersion objective (NA 1.2).
264

265 ## Live-cell imaging

266 Cells were arrested in G1 with as α-factor and subsequently released in low-fluorescence media
267 (LFM) containing 1.7 g/l yeast nitrogen base without ammonium sulfate, amino acids, folic acid and
268 riboflavin (MP-Biomedicals, 4030-512), and 1 g/l monosodium glutamate, supplemented with 2%
269 glucose and amino acids. Cells were left to settle on the bottom of concanavalin A-coated 96 well
270 glass bottom plates for 20-30 minutes inside the microscope incubator at 30°C before being imaged.
271 Images were captured every 5 min for 100-120 min.
272

273 ## Image analysis

274 Fluorescence intensity measurements were made from maximum intensity projections of image z-
275 stacks using FiJi (Schindelin et al., 2012). Integrated intensities were measured in a region of interest
276 drawn around spindles/kinetochores. Background correction was done by multiplying the mean
277 fluorescence of regions outside of the nucleus with the measured region's area and subtracting from
278 the measured integrated intensity. Linescan analysis was performed by drawing a line between the
279 centers of opposing SPB foci and measuring the fluorescence intensities along the line. Background
280 correction was done by subtracting the mean fluorescence measured at the cytoplasm. Binned
281 means were calculated for each strain. Cell cycle analyses were performed by classifying the cells
282 according to the spindle length, based on the Tub1-tagRFPT marker. (G1/S) spindles <1 µm ;
283 metaphase (1-2 µm), and anaphase (>2 µm).
284
285 ## Immunofluorescence

286 PGal1-Cdc20 cells were arrested in metaphase and fixed by adding formaldehyde to 3.7% (vol/vol)
287 and incubating while shaking at 30°C for 30 min. The fixed cells were washed once with PBS and then

288 twice with SP buffer (0.1 M KPO4, 1.2 M sorbitol, pH 7.5). The cells were resuspended in 500 µl SP
289 buffer with 0.1% β-mercaptoethanol and 10 µl of 20 mg/ml Zymoylase-20T (Seikagaku). The cells
290 were incubated with soft rotation for 20 min at room temperature (RT). The resulting spheroplasts
291 were then washed twice in SP buffer and permeabilized in blocking solution (3% BSA 0.1% Triton X-
292 100 in PBS) for 30 min at RT. The spheroplasts were immunostained in suspension. First, cells were
293 incubated with 1:1000 mouse monoclonal anti-FLAG M2 antibody (Sigma, F1804) in blocking buffer
294 for 1 hour at RT. Cells were washed three times in PBS and then incubated with 1:100 donkey anti-
295 mouse Alexa Fluor 647 antibody (ThermoFisher, A-31571) for 45 min at RT. Cells were washed three
296 times in PBS, seed in a glass-bottom imaging plate coated with Concanavalin A, and imaged.
297

298 Sample preparation for mass spectrometry analysis

299 Bik1-5xFlag PGal1-Cdc20 cells were arrested in metaphase. Briefly, cells were grown overnight in 50
300 ml YEP with 2% galactose and 2% raffinose. Cells were diluted in 2 L YEP with 2% and 2% raffinose
301 and grown at 30°C to OD_{600} = 1. Then, cells were spun down and resuspended in 2 L YEPD with 2%
302 glucose and arrested at 30°C for 2 h. Cells were spun down at 6000 rom at 4°C, washed with cold
303 dH_2O, and spun down at 6000 rpm at 4°C. The cell pellet was diluted in a few drops of lysis buffer (50
304 mM Tris, pH 8.0, 150 mM NaCl, 5% glycerol, 0.1% Triton X-100). The cell suspension was snap frozen
305 by pipetting the drops directly into liquid nitrogen. The frozen pellets were then lysed using a
306 Freezer/Mill (SPEX™ sample prep freezer/mill), using 10 rounds consisting of 2 min grinding at 14
307 rpm, 2 min cooling). The yeast pellets were diluted in buffer EB1 (40 mM sodium hepes, 300 mM
308 NaCl, 0.5% Triton X-100, 2 mM $MgCl_2$, 5% glycerol and protease and phosphatase inhibitors (1mM
309 PMSF, 1mM leupeptin, 1mM peptasin A, 10mM NaF, 1mM sodium pyrophosphatase, 1mm sodium
310 orthovanadate), and clarified by centrifugation at 10 000 g for 10 min at 4 °C. The cleared lysate was
311 incubated for 30 min with magnetic Dynabeads (Thermo Fisher Scientific) coupled with anti-FLAG M2
312 antibody (Sigma-Aldrich). The Dynabeads were washed three times with buffer A (25 mM sodium
313 Hepes, 2 mM $MgCl_2$, 0.1% EDTA, 0.1% Triton X-100, 5% glycerol, 150 mM NaCl, protease and

314 phosphatase inhibitors (1 mM PMSF, 1 mM leupeptin, 1 mM peptasin A, 10mM NaF, 1 mM sodium
315 pyrophosphatase, 1 mm sodium orthovanadate) and four times with buffer B (25 mM Hepes, pH 8.0,
316 and 150 mM KCl).
317
318 Protein on-beads digestion
319 Proteins bound to the Dynabeads were resuspended and washed with 500 µL of 50 mM ammonium
320 bicarbonate (AmBic), pH 8.0, twice. After incubation at room temperature for 15 min, 50 µL of 50
321 mM AmBic was added. Protein disulfide bonds were reduced with 5 µL of 200 mM dithiothreitol at
322 37°C for 45 min and alkylated with 5 µL of 600 mM iodoacetamide at room temperature in dark for
323 30 min. Tryptic digestion was started by adding 1 µg of trypsin and incubation at 37°C overnight,
324 followed by adding another 500 ng of trypsin and incubation at 30°C for 3 h. The digestion was
325 stopped with 5 µL concentrated formic acid. The samples were then cleaned on a C18 StageTip
326 (Thermo Scientific) and dried using a speedvac (MiVac, Thermo Scientific).
327
328 PRLC-MS/MS analysis
329 Chromatographic separations of peptides were performed on a 50 cm long C18 EASY-spray column
330 connected to an Easy nanoLC-1000 UPLC system (Thermo Fisher Scientific). The gradient was 4-25%
331 of solvent B (98% acetonitrile, 0.1% formic acid) in 50 min and 25-40%B in 10 min at a flow rate of
332 300 nl/min. An Orbitrap Fusion mass spectrometer (Thermo Scientific) analyzed the eluted peptides
333 that were ionized in a nano-Easy electrospray source. The survey mass spectrum was acquired at the
334 resolution of 120,000 in the range of *m/z* 350-1800. MS/MS data of precursors were obtained with
335 30% normalized collision energy by higher-energy collisional dissociation (HCD) for ions with charge
336 *z*=2-7 at a resolution of 30,000 in 3 s cycle time.
337
338 Data analysis

339 Mascot v 2.5.1 search engine (MatrixScience Ltd., UK) was used for protein identification with the
340 following search parameters: up to two missed cleavage sites for trypsin, peptide mass tolerance 10
341 ppm, 0.05 Da for the HCD fragment ions. Carbamidomethylation of cysteine was specified as a fixed
342 modification, whereas oxidation of methionine, deamidation of asparagine and glutamine were
343 defined as variable modifications.
344

345 ## Turbo-ID assay

346 Overnight cultures were diluted to OD_{600} = 0.2 in YEPD medium supplemented with 50 µM biotin and
347 grown at 30°C until they reached OD_{600} = 0.6 (4-5 h). Cells were pelleted and resuspended in RIPA
348 buffer (50 mM Tris-HCl, 150 mM NaCl, 1 mM EDTA, 0.1% SDS, 1% Triton X-100, 1.5 mM MgCl2, 0.4%
349 sodium deoxycholate, 1 mM DTT, 1 mM PMSF, 1 mM leupeptin and1 mM pepstatin A). The cells
350 were lysed using acid-washed glass beads and a bead-beater at 4°. To shear the DNA and RNA, the
351 cell lysate was sonicated, and then clarified by centrifugation. Clarified lysates were incubated with
352 100 µl of Streptavidin-Sepharose beads (GE Healthcare; 17-5113-01) for 3 h at 40°C. The beads were
353 then washed once with wash buffer (50mM Tris-HCl, 2% SDS) and three times with RIPA buffer. The
354 purified proteins were eluted with 4 x Laemmli buffer containing 25 µM biotin and 10% β-
355 mercaptoethanol, for 15 min at 95°C. The whole cell extract or pull-down samples were separated by
356 SDS-PAGE, and the proteins were transferred to a PVDF membrane (BioRad) followed by and
357 standard immunoblotting. Primary (monoclonal anti-FLAG M2 antibody (Sigma-Aldrich, F3165,
358 diluted 1:5000); c-Myc rabbit polyclonal antibody (Santa Cruz Biotechnology; sc-789, diluted 1:5000);
359 anti-Pgk1 mouse monoclonal antibody (Invitrogen, 45925, diluted 1:5000), and secondary anti-
360 mouse IgG peroxidase antibody, (Sigma, A9044, diluted 1:50000) were used. HRP conjugated
361 secondary antibodies were detected with Femto ECL (ThermoFisher Scientific).
362

Acknowledgements

We thank C. Björkegren (Karolinska Institutet, Sweden) for reagents, and C. Boone and Z. Li for help with construction of deletion mutants and critical reading of this manuscript. Microscopy was performed at the Live Cell Imaging Core facility/Nikon Center of Excellence, at the Karolinska Institutet, supported by grants from the Swedish Research Council, KI infrastructure, and Centre for Innovative Medicine. The BioImage Informatics Facility at SciLifeLab, National Microscopy Infrastructure (VR-RFI 2019-00217), and recipient of the Chan-Zuckerberg Initiative, assisted in the image analysis. Protein identification and quantification were carried out by the Proteomics Biomedicum core facility, Karolinska Institutet. This work was supported by grants from the Swedish Council (VR-NT 2017-04536), and STINT (Mobility Grant for Internationalization, MG2019-8484) to V.M.B. The authors declare no competing financial interests.

References

Akhmanova, A., & Steinmetz, M. O. (2010). Microtubule +TIPs at a glance. In *Journal of Cell Science* (Vol. 123, Issue 20). https://doi.org/10.1242/jcs.062414

Berlin, V., Styles, C. A., & Fink, G. R. (1990). BIK1, a protein required for microtubule function during mating and mitosis in Saccharomyces cerevisiae, colocalizes with tubulin. *Journal of Cell Biology*, *111*(6 I). https://doi.org/10.1083/jcb.111.6.2573

Branon, T. C., Bosch, J. A., Sanchez, A. D., Udeshi, N. D., Svinkina, T., Carr, S. A., Feldman, J. L., Perrimon, N., & Ting, A. Y. (2018). Efficient proximity labeling in living cells and organisms with TurboID. *Nature Biotechnology*, *36*(9). https://doi.org/10.1038/nbt.4201

Britto, M., Goulet, A., Rizvi, S., Von Loeffelholz, O., Moores, C. A., & Cross, R. A. (2016). Schizosaccharomyces pombe kinesin-5 switches direction using a steric blocking mechanism. *Proceedings of the National Academy of Sciences of the United States of America*, *113*(47). https://doi.org/10.1073/pnas.1611581113

388 Carvalho, P., Gupta, M. L., Hoyt, M. A., & Pellman, D. (2004). Cell cycle control of kinesin-mediated
389 transport of Bik1 (CLIP-170) regulates microtubule stability and dynein activation.
390 *Developmental Cell*, *6*(6). https://doi.org/10.1016/j.devcel.2004.05.001
391 Caudron, F., Andrieux, A., Job, D., & Boscheron, C. (2008). A new role for kinesin-directed transport of
392 Bik1p (CLIP-170) in Saccharomyces cerevisiae. *Journal of Cell Science*, *121*(9).
393 https://doi.org/10.1242/jcs.023374
394 Dudziak, A., Engelhard, L., Bourque, C., Klink, B. U., Rombaut, P., Kornakov, N., Jänen, K., Herzog, F.,
395 Gatsogiannis, C., & Westermann, S. (2021). Phospho-regulated Bim1/EB1 interactions trigger
396 Dam1c ring assembly at the budding yeast outer kinetochore. *The EMBO Journal*, *40*(18).
397 https://doi.org/10.15252/embj.2021108004
398 Gardner, M. K., Bouck, D. C., Paliulis, L. V., Meehl, J. B., O'Toole, E. T., Haase, J., Soubry, A., Joglekar,
399 A. P., Winey, M., Salmon, E. D., Bloom, K., & Odde, D. J. (2008). Chromosome Congression by
400 Kinesin-5 Motor-Mediated Disassembly of Longer Kinetochore Microtubules. *Cell*, *135*(5).
401 https://doi.org/10.1016/j.cell.2008.09.046
402 Gardner, M. K., Pearson, C. G., Sprague, B. L., Zarzar, T. R., Bloom, K., Salmon, E. D., & Odde, D. J.
403 (2005). Tension-dependent Regulation of Microtubule Dynamics at Kinetochores Can Explain
404 Metaphase Congression in Yeast. *Molecular Biology of the Cell*, *16*(8), 3764–3775.
405 https://doi.org/10.1091/mbc.e05-04-0275
406 Gerson-Gurwitz, A., Thiede, C., Movshovich, N., Fridman, V., Podolskaya, M., Danieli, T., Lakämper, S.,
407 Klopfenstein, D. R., Schmidt, C. F., & Gheber, L. (2011). Directionality of individual kinesin-5 Cin8
408 motors is modulated by loop 8, ionic strength and microtubule geometry. *EMBO Journal*,
409 *30*(24). https://doi.org/10.1038/emboj.2011.403
410 Hoyt, M. A., He, L., Kek Khee Loo, & Saunders, W. S. (1992). Two Saccharomyces cerevisiae kinesin-
411 related gene products required for mitotic spindle assembly. *Journal of Cell Biology*, *118*(1).
412 https://doi.org/10.1083/jcb.118.1.109
413 Kops, G. J. P. L., Saurin, A. T., & Meraldi, P. (2010). Finding the middle ground: How kinetochores

power chromosome congression. In *Cellular and Molecular Life Sciences* (Vol. 67, Issue 13). https://doi.org/10.1007/s00018-010-0321-y

Kosugi, S., Hasebe, M., Tomita, M., & Yanagawa, H. (2008). Nuclear export signal consensus sequences defined using a localization-based yeast selection system. *Traffic*, *9*(12). https://doi.org/10.1111/j.1600-0854.2008.00825.x

Kotwaliwale, C. V., Frei, S. B., Stern, B. M., & Biggins, S. (2007). A Pathway Containing the Ipl1/Aurora Protein Kinase and the Spindle Midzone Protein Ase1 Regulates Yeast Spindle Assembly. *Developmental Cell*, *13*(3). https://doi.org/10.1016/j.devcel.2007.07.003

Larochelle, M., Bergeron, D., Arcand, B., & Bachand, F. (2019). Proximity-dependent biotinylation mediated by TurboID to identify protein-protein interaction networks in yeast. *Journal of Cell Science*, *132*(11). https://doi.org/10.1242/jcs.232249

Lin, H., De Carvalho, P., Kho, D., Tai, C. Y., Pierre, P., Fink, G. R., & Pellman, D. (2001). Polyploids require Bik1 for kinetochore-microtubule attachment. *Journal of Cell Biology*, *155*(7). https://doi.org/10.1083/jcb.200108119

Longtine, M. S., McKenzie, A., Demarini, D. J., Shah, N. G., Wach, A., Brachat, A., Philippsen, P., & Pringle, J. R. (1998). Additional modules for versatile and economical PCR-based gene deletion and modification in Saccharomyces cerevisiae. *Yeast*, *14*(10). https://doi.org/10.1002/(SICI)1097-0061(199807)14:10<953::AID-YEA293>3.0.CO;2-U

Maiato, H., Gomes, A. M., Sousa, F., & Barisic, M. (2017). Mechanisms of chromosome congression during mitosis. In *Biology* (Vol. 6, Issue 1). https://doi.org/10.3390/biology6010013

Marco, E., Dorn, J. F., Hsu, P. H., Jaqaman, K., Sorger, P. K., & Danuser, G. (2013). S. cerevisiae chromosomes biorient via gradual resolution of syntely between S phase and anaphase. *Cell*, *154*(5). https://doi.org/10.1016/j.cell.2013.08.008

Markus, S. M., Omer, S., Baranowski, K., & Lee, W. L. (2015). Improved Plasmids for Fluorescent Protein Tagging of Microtubules in Saccharomyces cerevisiae. *Traffic*, *16*(7). https://doi.org/10.1111/tra.12276

440 Miller, R. K., D'Silva, S., Moore, J. K., & Goodson, H. V. (2006). The CLIP-170 Orthologue Bik1p and
441 Positioning the Mitotic Spindle in Yeast. In *Current Topics in Developmental Biology* (Vol. 76).
442 https://doi.org/10.1016/S0070-2153(06)76002-1
443 Molk, J. N., Salmon, E. D., & Bloom, K. (2006). Nuclear congression is driven by cytoplasmic
444 microtubule plus end interactions in S. cerevisiae. *Journal of Cell Biology*, *172*(1).
445 https://doi.org/10.1083/jcb.200510032
446 Moore, J. K., D'Silva, S., & Miller, R. K. (2006). The CLIP-170 homologue Bik1p promotes the
447 phosphorylation and asymmetric localization of Kar9p. *Molecular Biology of the Cell*, *17*(1).
448 https://doi.org/10.1091/mbc.E05-06-0565
449 O'Toole, E. T., Winey, M., & McIntosh, J. R. (1999). High-voltage electron tomography of spindle pole
450 bodies and early mitotic spindles in the yeast Saccharomyces cerevisiae. *Molecular Biology of*
451 *the Cell*, *10*(6). https://doi.org/10.1091/mbc.10.6.2017
452 Pandey, H., Reithmann, E., Goldstein-Levitin, A., Al-Bassam, J., Frey, E., & Gheber, L. (2021). Drag-
453 induced directionality switching of kinesin-5 Cin8 revealed by cluster-motility analysis. *Science*
454 *Advances*, *7*(6). https://doi.org/10.1126/sciadv.abc1687
455 Pearson, C. G., Gardner, M. K., Paliulis, L. V., Salmon, E. D., Odde, D. J., & Bloom, K. (2006). Measuring
456 nanometer scale gradients in spindle microtubule dynamics using model convolution
457 microscopy. *Molecular Biology of the Cell*, *17*(9). https://doi.org/10.1091/mbc.E06-04-0312
458 Peterson, J. B., & Ris, H. (1976). Electron microscopic study of the spindle and chromosome
459 movement in the yeast Saccharomyces cerevisiae. *Journal of Cell Science*, *22*(2).
460 Powers, A. F., Franck, A. D., Gestaut, D. R., Cooper, J., Gracyzk, B., Wei, R. R., Wordeman, L., Davis, T.
461 N., & Asbury, C. L. (2009). The Ndc80 Kinetochore Complex Forms Load-Bearing Attachments to
462 Dynamic Microtubule Tips via Biased Diffusion. *Cell*, *136*(5).
463 https://doi.org/10.1016/j.cell.2008.12.045
464 Roberts, A. J., Goodman, B. S., & Reck-Peterson, S. L. (2014). Reconstitution of dynein transport to
465 the microtubule plus end by kinesin. *ELife*, *3*. https://doi.org/10.7554/elife.02641

466 Roostalu, J., Hentrich, C., Bieling, P., Telley, I. A., Schiebel, E., & Surrey, T. (2011). Directional
467 switching of the kinesin Cin8 through motor coupling. *Science*, *332*(6025).
468 https://doi.org/10.1126/science.1199945
469 Roux, K. J., Kim, D. I., Raida, M., & Burke, B. (2012). A promiscuous biotin ligase fusion protein
470 identifies proximal and interacting proteins in mammalian cells. *Journal of Cell Biology*, *196*(6).
471 https://doi.org/10.1083/jcb.201112098
472 Schindelin, J., Arganda-Carreras, I., Frise, E., Kaynig, V., Longair, M., Pietzsch, T., Preibisch, S., Rueden,
473 C., Saalfeld, S., Schmid, B., Tinevez, J. Y., White, D. J., Hartenstein, V., Eliceiri, K., Tomancak, P., &
474 Cardona, A. (2012). Fiji: An open-source platform for biological-image analysis. In *Nature*
475 *Methods* (Vol. 9, Issue 7). https://doi.org/10.1038/nmeth.2019
476 Sprague, B. L., Pearson, C. G., Maddox, P. S., Bloom, K. S., Salmon, E. D., & Odde, D. J. (2003).
477 Mechanisms of microtubule-based kinetochore positioning in the yeast metaphase spindle.
478 *Biophysical Journal*, *84*(6). https://doi.org/10.1016/S0006-3495(03)75087-5
479 Su, X., Qiu, W., Gupta, M. L., Pereira-Leal, J. B., Reck-Peterson, S. L., & Pellman, D. (2011).
480 Mechanisms Underlying the Dual-Mode Regulation of Microtubule Dynamics by Kip3/Kinesin-8.
481 *Molecular Cell*, *43*(5). https://doi.org/10.1016/j.molcel.2011.06.027
482 Sung, M. K., & Huh, W. K. (2007). Biomolecular fluorescence complementation analysis system for in
483 vivo detection of protein-protein interaction in Saccharomyces cerevisiae. *Yeast*, *24*(9).
484 https://doi.org/10.1002/yea.1504
485 Suzuki, A., Badger, B. L., Haase, J., Ohashi, T., Erickson, H. P., Salmon, E. D., & Bloom, K. (2016). How
486 the kinetochore couples microtubule force and centromere stretch to move chromosomes.
487 *Nature Cell Biology*, *18*(4). https://doi.org/10.1038/ncb3323
488 Suzuki, A., Gupta, A., Long, S. K., Evans, R., Badger, B. L., Salmon, E. D., Biggins, S., & Bloom, K. (2018).
489 A Kinesin-5, Cin8, Recruits Protein Phosphatase 1 to Kinetochores and Regulates Chromosome
490 Segregation. *Current Biology*, *28*(17). https://doi.org/10.1016/j.cub.2018.08.038
491 Tytell, J. D., & Sorger, P. K. (2006). Analysis of kinesin motor function at budding yeast kinetochores.

492 *Journal of Cell Biology*, *172*(6). https://doi.org/10.1083/jcb.200509101

493 Varga, V., Helenius, J., Tanaka, K., Hyman, A. A., Tanaka, T. U., & Howard, J. (2006). Yeast kinesin-8
494 depolymerizes microtubules in a length-dependent manner. *Nature Cell Biology*, *8*(9).
495 https://doi.org/10.1038/ncb1462

496 Wargacki, M. M., Tay, J. C., Muller, E. G., Asbury, C. L., & Davis, T. N. (2010). Kip3, the yeast kinesin-8,
497 is required for clustering of kinetochores at metaphase. *Cell Cycle*, *9*(13).
498 https://doi.org/10.4161/cc.9.13.12076

499 Winey, M., Mamay, C. L., O'Toole, E. T., Mastronarde, D. N., Giddings, T. H., McDonald, K. L., &
500 McIntosh, J. R. (1995). Three-dimensional ultrastructural analysis of the Saccharomyces
501 cerevisiae mitotic spindle. *Journal of Cell Biology*, *129*(6).
502 https://doi.org/10.1083/jcb.129.6.1601

503 Winey, M., & O'Toole, E. T. (2001). The spindle cycle in budding yeast. In *Nature Cell Biology* (Vol. 3,
504 Issue 1). https://doi.org/10.1038/35050663

505 Xiang, X. (2018). Nuclear movement in fungi. In *Seminars in Cell and Developmental Biology* (Vol. 82).
506 https://doi.org/10.1016/j.semcdb.2017.10.024

507

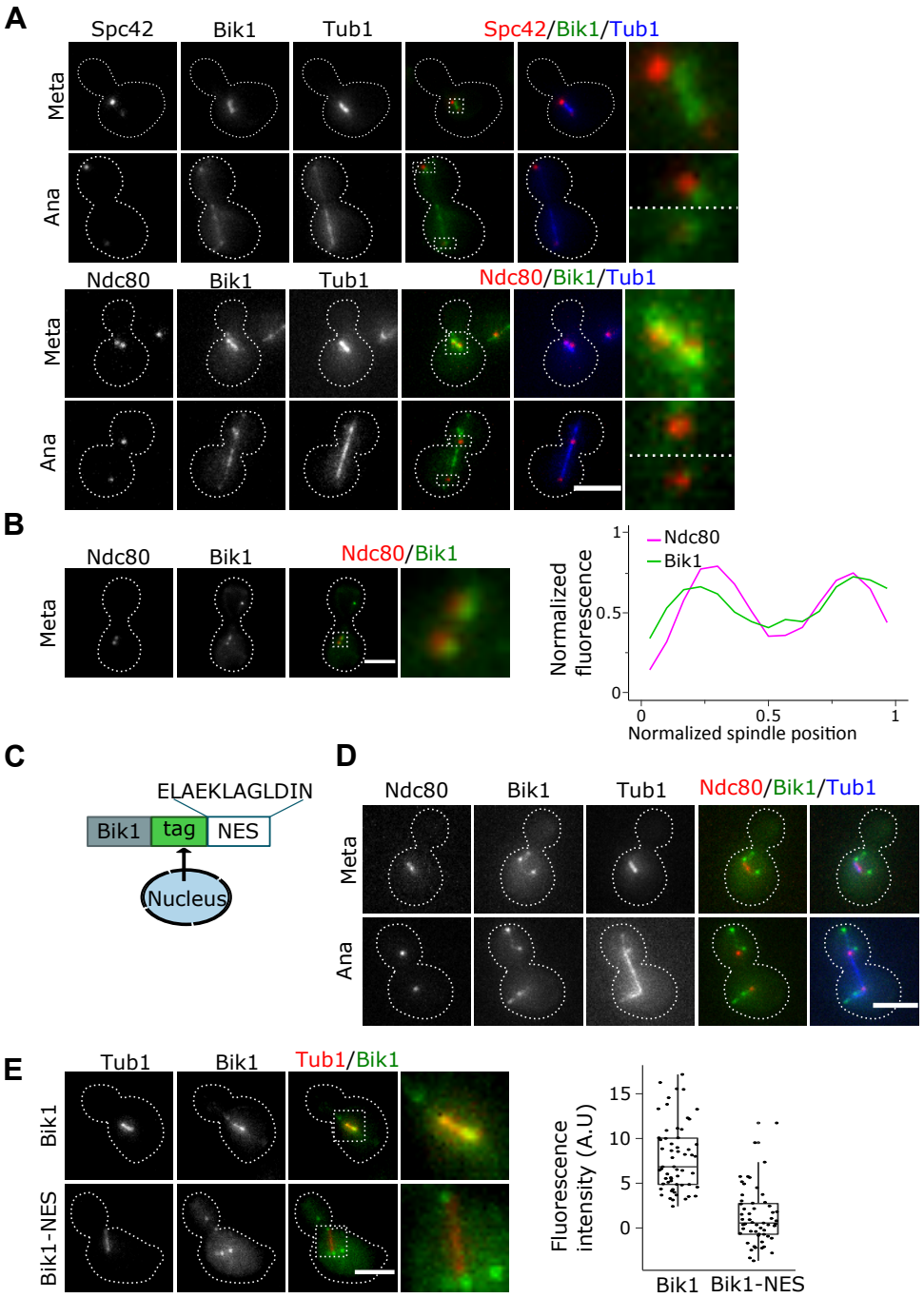

Figure 1. Bik1 localizes to kinetochores in a cell-cycle dependent manner. (A) Representative images of Bik1-sfGFP (green) localization in cycling cells expressing mTurquoise-Tub1 (blue) and Spc42-tagRFP-T (red, top panel), and Nc80-tagRFP-T (red, lower panel). Dashed boxes show area enlarged in the rightmost images. (B) Left panel: Representative images of Bik1-sfGFP (green) localization in pGal1-Cdc20 metaphase-arrested cells expressing Nc80-tagRFP-T. Right panel: Line scan analysis shows the distribution of Bik1-sfGFP and kinetochores (Ndc80-tagRFP-T) in metaphase arrested cells. For each cell, the fluorescence intensity was measured along a line drawn between the kinetochore foci and normalized relative to the maximum value, and the mean values are shown (n=26 cells). Dashed boxes show area enlarged in the rightmost images. (C) Cartoon showing the design of Bik1-NES. In short, a strong nuclear export signal (NES) was fused to Bik1-sfGFP or Bik1-5xFlag to promote nuclear export. (D) Representative images of Bik1-sfGFP-NES (green) localization in cycling cells expressing mTurquoise-Tub1 (blue) and Ndc80-tagRFPT (red). (E) Quantification of Bik1-sfGFP or Bik1-sfGFP-NES localization in metaphase cells. Bik1-sfGFP and Bik1-sfGFP-NES cells expressing mRuby2-Tub1 were arrested in G1 with α-factor and subsequently released in fresh media. Cells were fixed every 10 minutes for 120 minutes. Left: Representative cells at metaphase. Time after release = 40 min (Bik1-sfGFP), and 50 min (Bik1-sfGFP-NES). Right: Boxplots of the integrated fluorescence intensity of Bik1-sfGFP and Bik1-sfGFP-NES at the spindle (mRuby2-Tub1) in metaphase cells (n=59 cells for Bik1-sfGFP and 55 for Bik1-sfGFP-NES). Dashed boxes show area enlarged in the rightmost images. All images shown are maximum intensity projections of Z-stacks (9 µm, 1 µm steps). Dashed lines represent the cell outlines based on bright field images. All scale bars, 4 µm.

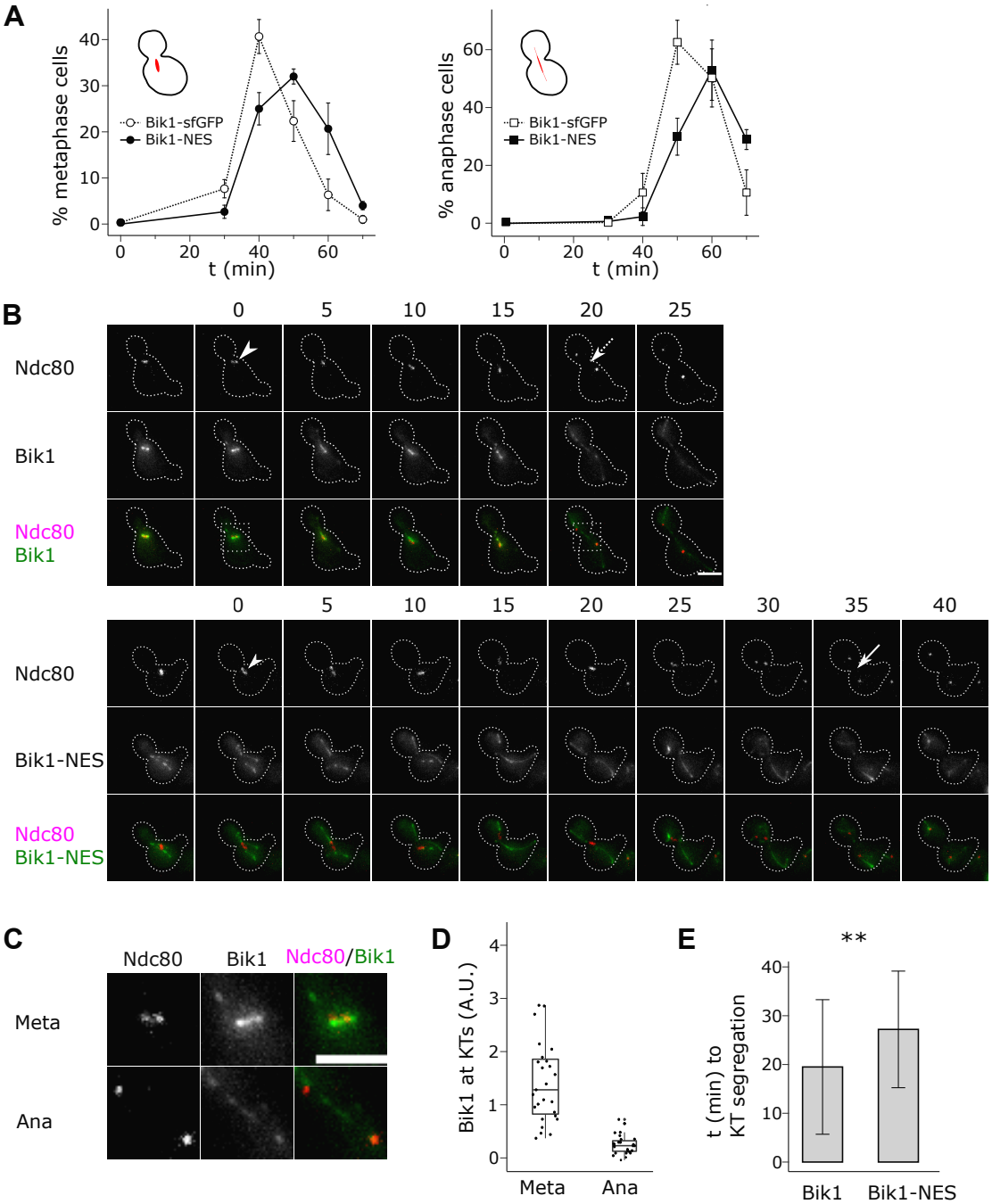

Figure 2. Bik1-NES delays spindle elongation at metaphase/anaphase transition. (A) Cells from (1E) were scored for cell cycle progression based on bud size and spindle length (mRuby-Tub1). Error bars represent mean ± sd (n=3 independent experiments, each experiment with 100 cells each timepoint for each strain (Bik1-sfGFP and Bik1-sfGFP-NES) analysed per experiment). (B-E) Time-lapse imaging of cells expressing Bik1-sfGFP or Bik1-sfGFP-NES (green) and Ndc80-tagRFP-T (red). Cells were arrested in G1 with α-factor and subsequently released in fresh medium under the microscope. Images were taken at 5 min intervals. (B) Representative time-lapse images. Arrowheads indicate the appearance of separated kinetochore clusters. Arrows indicate segregated kinetochores in mother/bud. The time (min) elapsed from appearance of separated kinetochore clusters is indicated by the numbers above the frames. Dashed boxes show area enlarged in (C). Images shown are maximum intensity projections of Z-stacks (9 µm, 1 µm steps). Scale bar, 4 µm. (C) Zoomed-in images from the dashed areas of (B), showing the kinetochores (Ndc80-tagRFP-T) at metaphase and anaphase. (D) Boxplots of the integrated Bik1-sfGFP fluorescence intensity at kinetochores (Ndc80-tagRFP-T) at metaphase (meta) and anaphase (ana) (n= 27 cells). (E) Quantification of average time from the appearance of separated kinetochore clusters to segregated kinetochores in mother/bud in Bik1-sfGFP and Bik1-sfGFP-NES cells. We performed two independent experiments and pooled the data. Error bars represent mean ± sd (n= 59 cells for Bik1-sfGFP and 57 for Bik1-sfGFP-NES, p-value = 0.001691 using Welch Two Sample t-test (two-sided)).

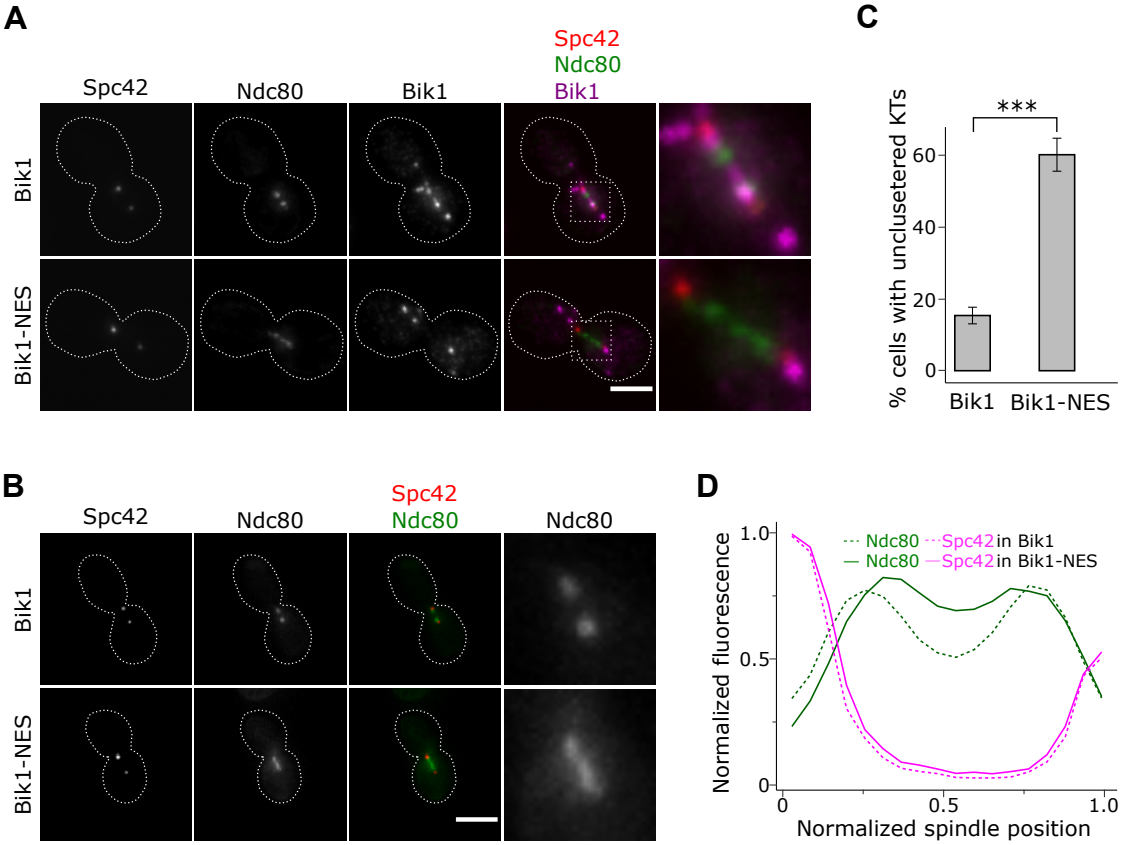

Figure 3. Nuclear Bik1 is needed for kinetochore clustering at metaphase. (A) Representative immunofluorescence staining for Bik1-5xFlag and Bik1-5xFlag-NES (magenta) in metaphase arrested pGal1-Cdc20 cells expressing Spc42-sfGFP (red) and Ndc80-TagRFP-T (green). Images shown are maximum intensity projections of Z-stacks (4.95 µm, 0.3 µm steps). Dashed boxes show area enlarged in the rightmost images. Scale bar, 4 µm. (B) Representative images of Bik1-5xFlag and Bik1-5xFlag-NES arrested as in (A), including zoomed-in images of the kinetochores (Ndc80-sfGFP). Images shown are maximum intensity projections of Z-stacks (8.7 µm, 0.3 µm steps). Scale bar, 4 µm. (C) Quantification of kinetochore (Ndc80-tagRFPT) unclustered phenotype in Bik1-5xFlag and Bik-5xFlag-NES cells arrested in metaphase as shown in (B). Error bars represent mean ± sd (n=3 independent experiments, with 100 cells for each strain (Bik1-5xFlag and Bik1-5xFlag-NES). p=0.0006884 using Welch Two Sample t-test (two-sided). (D) Line scan analysis shows the distribution of kinetochores (Ndc80sfGFP) and spindle pole bodies (SPBs, Spc42-tagRFP-T) in metaphase arrested cells. For each cell, the fluorescence intensity was measured along lines drawn between the SPBs (Spc42-TagRFP-T) and normalized relative to the maximum value. Mean values are shown (n=100 cells for each strain (Bik1-5xFlag and Bik1-5xFlag-NES).

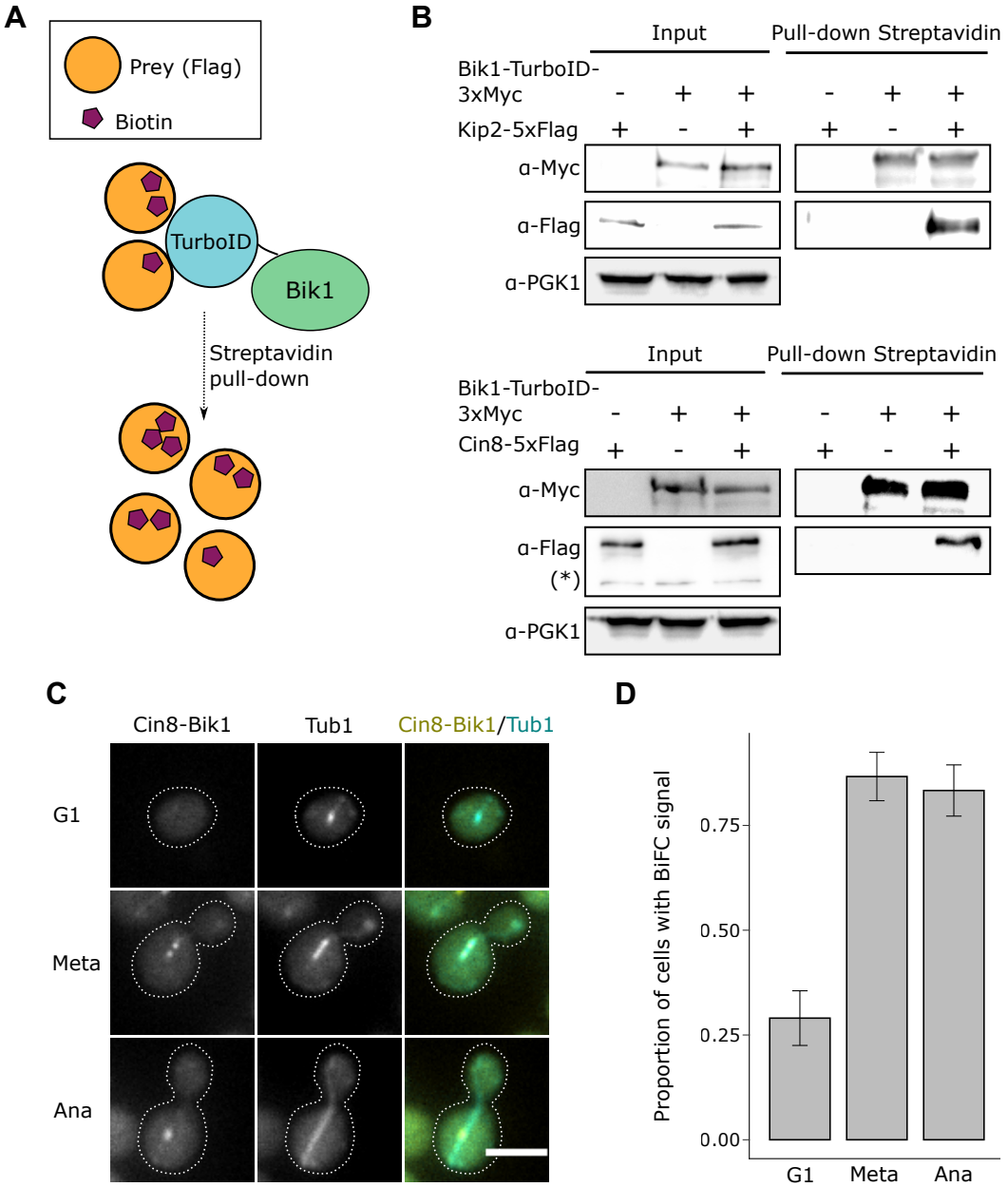

Figure 4. Bik1 interacts with Cin8 at metaphase. (A-B) Identification of Cin8 as a Bik1 interaction partner using TurboID. Cartoon outlining the principle of the TurboID assay. Briefly, a biotin ligase was fused to endogenous Bik1 (Bik1-TurboID) in cells expressing the protein of interest tagged with Flag (Prey). Biotinylated substrates were purified using streptavidin beads, and inputs and pull-down lysates were analyzed by immunoblot for the indicated proteins. (B) Western blot analysis of total cell extracts (input) and streptavidin pull-downs prepared from Bik1-TurboID-3xmyc cells expressing Kip2-5xFlag or Cin8-5xFlag as prey, and control strains, using anti-Myc (top) and anti-Flag (bottom) antibodies. (*) unspecific band. (C-D) Bimolecular fluorescence complementation (BiFC) analysis of Bik1 and Cin8 interaction. (C) Representative images of cycling cells expressing Bik1-VN and Cin8-VC in G1, metaphase and anaphase. Images shown are single focal planes. (D) Proportion of cells in (C) with BIFC signal based on Venus fluorescence. Error bars represent mean ± sd (n= 3 independent experiments, with 50 cells analyzed in each cell cycle phase (G1, metaphase and anaphase) per experiment.

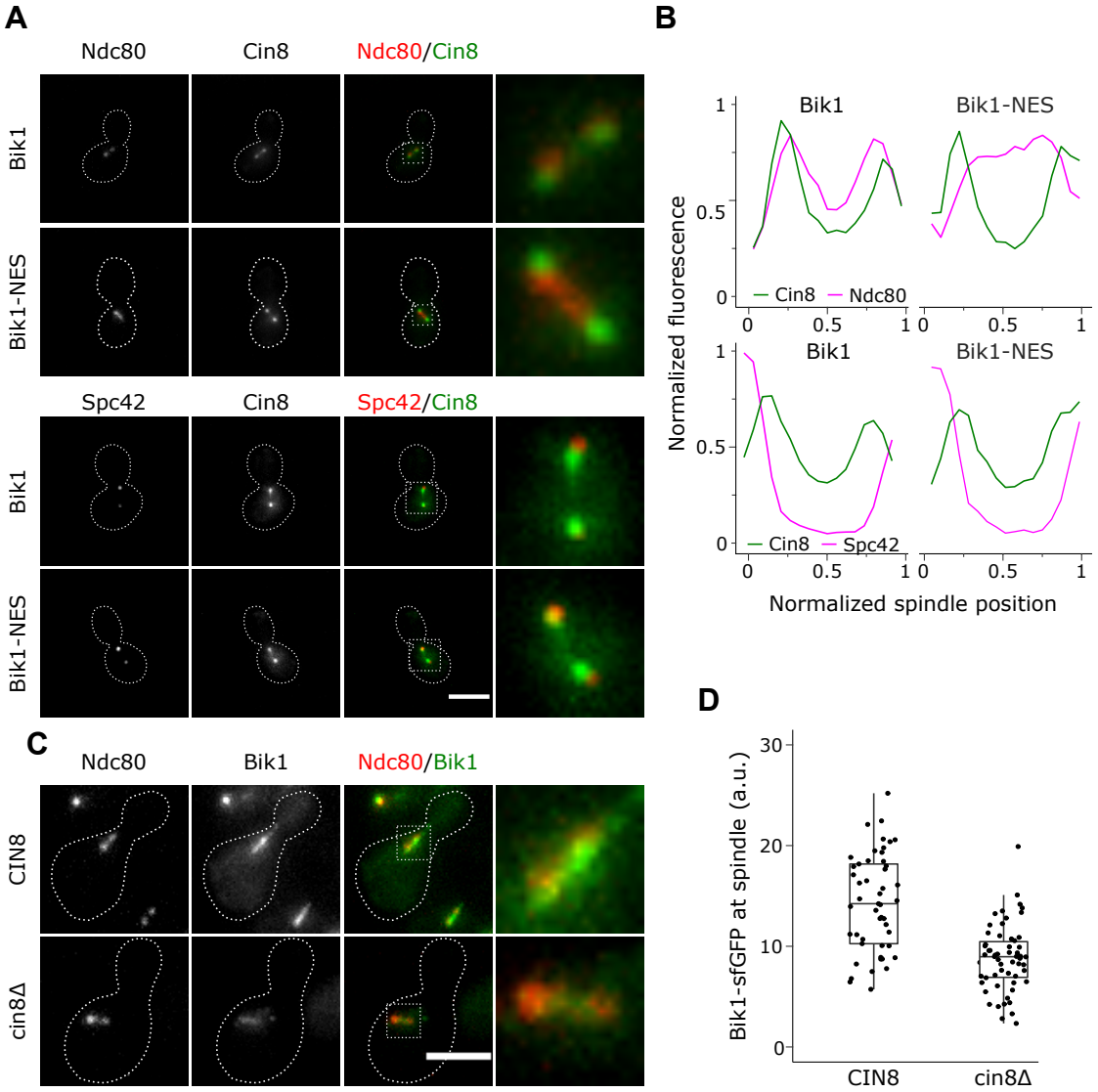

Figure 5. Dependence of Cin8 and Bik1 to localize to the spindle. (A-B) Cin8 localizes at the spindle in Bik1-NES cells but does not co-localize with unclustered kinetochores. (A) Cin8 localization at the metaphase spindle does not require nuclear Bik1. Representative images of pGal1-Cdc20 cells arrested in metaphase expressing Bik1-5xFlag or Bik1-5xFlag-NES, Cin8-sfGFP, and the markers Ndc80-TagRFP-T (top panel) or Spc42-TagRFP-T (lower panel). Images shown are maximum intensity projections of Z-stacks (8.7 µm, 0.3 µm steps). Dashed boxes show area enlarged in the rightmost images. Scale bar, 4 µm. (B) Line scan analysis of Cin8 distribution (Cin8-sfGFP) in metaphase arrested cells). Top panel: Cin8 distribution relative to the kinetochores (Ndc80-tagRFP-T). For each cell, the fluorescence intensities of Cin8-sfGFP and Ndc80-tagRFPT was measured along lines drawn between the SPBs and normalized relative to the maximum values, mean values are shown (n= 25 cells for BIK1 and 25 for Bik1-5xFlag-NES). Low panel: Cin8 distribution relative to the SPBs (Spc42-tagRFP-T). For each cell, the fluorescence intensity of Cin8-sfGFP and Spc42-tagRFPT was measured along a line drawn between the SPBs and normalized relative to the maximum value. Mean values are shown (n= 25 cells for Bik1-5xFlag and 26 for Bik1-5xFlag-NES). (C) Cin8 is needed for Bik1-sfGFP localization at kinetochores. CIN8 and cin8Δ cells expressing Bik1-sfGFP and Ndc80-TagRFP-T were arrested in G1 using α-factor, released in fresh media at 25°C and fixed every 10 minutes for 130 minutes. Left: Representative images of cells in metaphase (CIN8, 60 min after release; cin8Δ, 110 min after release). Images shown are maximum intensity projections of Z-stacks (6.6 µm, 0.6 µm steps). Dashed boxes show area enlarged in the rightmost images. Scale bar, 4 µm.

(D) Boxplots of the integrated fluorescence intensity of Bik1-sfGFP at the spindle (based on Ndc80-TagRFP-T localization) in metaphase cells (n=100 cells for each strain (CIN8 and cin8 Δ).

Table 1. A subset of the protein interactors of Bik1-FLAG (See Data S1 for a complete list).

Name	% Coverage	Unique peptides
STU2	72.33	104
BIM1	67.00	21
CIN8	50.67	46
KIP2	49.33	28
KAR9	47.33	26
KIP1	38.67	28
KAR3	38.67	23
CIK1	22.67	10
VIK1	21.00	10
KIP3	15.33	6

Table S1. Strains used in this study. All strains are derived from BY4741

Strain	Genotype
VMB-212	MATα BIK1-sfGFP:Ura3 SPC42-tagRFP-T:KanMX Leu2:HIS3p:mTurquoise2-TUB1
VMB-154	MATα BIK1-sfGFP:Ura3 NDC80-tagRFP-T:KanMX Leu2:HIS3p:mTurquoise2-TUB1
VMB-185	MATa BIK1-sfGFP:Ura3 NDC80-tagRFP-T:KanMX
VMB-293	MATa NatN2:PGAL1-CDC20 BIK1-sfGFP:Ura3 NDC80-tagRFP-T:KanMX
VMB-156	MATα BIK1-sfGFP-NES:NatMX NDC80-tagRFP-T:KanMX Leu2:HIS3p:mTurquoise2-TUB1
VMB-166	MATa BIK1-sfGFP:Ura3 Leu2:HIS3p:mRuby2-TUB1
VMB-209	MATa BIK1-sfGFP-NES:NatMX Leu2:HIS3p:mRuby2-TUB1
VMB-455	MATa HygroMX:PGAL1-CDC20 BIK1-5xFlag-NES:NatMX NDC80-sfGFP:Ura3 SPC42-tagRFP-T:KanMX
VMB-458	MATa HygroMX:PGAL1-CDC20 BIK1-5xFlag:NatMX NDC80-sfGFP:Ura3 SPC42-tagRFP-T:KanMX
VMB-433	MATa KIP2-5xFlag:KanMX
VMB-422	MATa BIK1-TurboID-3xMyc:NatMX
VMB-431	MATa BIK1-TurboID-3xMyc:NatMX KIP2-5xFlag:KanMX
VMB-393	MATa CIN8-5xFlag:KanMX
VMB-428	MATa BIK1-TurboID-3xMyc:NatMX CIN8-5xFlag:KanMX
VMB-448	MATa HygroMX:PGAL1-CDC20 CIN8-sfGFP:Ura3 NDC80-tagRFP-T:KanMX
VMB-453	MATa HygroMX:PGAL1-CDC20 BIK1-5xFlag-NES:NatMX CIN8-sfGFP:Ura3 NDC80-tagRFP-T:KanMX
VMB-459	MATa HygroMX:PGAL1-CDC20 BIK1-5xFlag:NatMX CIN8-sfGFP:Ura3 SPC42-tagRFP-T:KanMX
VMB-457	MATa HygroMX:PGAL1-CDC20 BIK1-5xFlag-NES:NatMX CIN8-sfGFP:Ura3 SPC42-tagRFP-T:KanMX
VMB-308	MATa BIK1-sfGFP:Ura3 cin8Δ:natMX NDC80-tagRFP-T:KanMX
VMB-288	MATa NatN2:PGAL1-CDC20 BIK1-5xFlag:KanMX
VMB-494	MATa BIK1-VN173:His3MX CIN8-VC155:KanMX Leu2:HIS3p:mTurquoise2-TUB1

Table S2. Plasmids used in this study

Plasmid	Relevant insert	Source
p44873	pFA6a-link-yosuperfolderGFP-CaURA3	Gift from Wendell Lim & Kurt Thorn (Addgene: 44873) PMID: 23844123
p44906	pFA6a-link-yoTagRFP-T-Kan	Gift from Wendell Lim & Kurt Thorn (Addgene: 44906) PMID: 23844123
p50641	pHIS3p:mTurquoise2-Tub1+3'UTR::LEU2	Gift from Wei-Lih Lee (Addgene: 50641) PMID: 25711127
p50645	pHIS3p:mRuby2-Tub1+3'UTR::LEU2	Gift from Wei-Lih Lee (Addgene: 50645) PMID: 25711127
pYM-N23	ScGAL1 promoter::pAgTEF-nat-tScADH1	PCR-Toolbox Knop (Euroscarf) MID: 15334558
p15983	pFA6a-5xFlag-KanMX6	Gift from Eishi Noguchi (Addgene: 15983) PMID: 18729046
	pFA6a-5xFlag-NatMX6	This study (subclonned from p15983)
pFB1434	pFA6a-Turbo-ID-3Myc-NatMX6	Gift from François Bachand (Addgene: 126050) PMID: 31064814
P30555	pFA6a-VN-His3MX6	Gift from Sung MK & Huh WK. (Euroscarf) PMID: 17534848
P30560	pFA6a-VC-kanMX6	Gift from Sung MK & Huh WK. (Euroscarf) PMID: 17534848